Measurement 121 (2018) 83–95

Contents lists available at ScienceDirect

Measurement

journal homepage: www.elsevier.com/locate/measurement

Development of a prediction model for estimating tractor engine torque based on soft computing and low cost sensors

Majid Rajabi-Vandechali, Mohammad Hossein Abbaspour-Fard*, Abbas Rohani

Department of Biosystems Engineering, Ferdowsi University of Mashhad, Mashhad, Iran

ARTICLE INFO

Keywords:
ANFIS
RBF
Engine torque
Tractor

ABSTRACT

Torque estimation needs intensive efforts and costly sensors. In this research, a model was proposed based on soft computing to estimate the ITM285 tractor engine torque using some low cost sensors. To this end, two models including the radial basis function (RBF) neural network and adaptive neuro fuzzy inference system (ANFIS) were used. Thirteen training algorithms were examined to train the RBF. These algorithms were compared using three statistical methods, namely k-fold cross validation, completely randomized design (CRD) and least significant difference (LSD). Moreover, three methods, namely grid partitioning (GP), sub-clustering (SC) and fuzzy c-means (FCM), were used to construct the fuzzy inference system (FIS). However, the FCM was the most suitable method. The sensitivity analysis showed that only measuring engine speed, fuel mass flow and exhaust gas temperature was sufficient for proper engine torque estimation. The RBF had a better performance (R^2 = 0.99, RMSE = 0.5 and EF = 0.99) than the ANFIS and hence, was suggested for estimating the engine torque.

1. Introduction

Diesel engines are widely used in vehicles, ships, power generators, military equipment, heavy industries and agricultural machinery, especially tractors. They offer a better fuel to power conversion efficiency than spark ignition (SI) types [1] and the lower volatility of their fuel makes them safer to handle [2]. The engine is the heart of such equipment and thus, keeping it in a good working condition is vital for a good overall efficiency [3]. Most of agricultural implements with active tillage tools (e.g., rotary tiller, power harrow), balers, choppers, mowers, threshing machinery, sprayers, spreaders, etc., are powered by a power-take-off (PTO) shaft. On the go estimation of rotary power consumption in these implements is very important for the farm power management purpose. Monitoring the tractor engine load is crucial for engineers to design implements as well as for farm experts to manage machinery and make proper decisions. Furthermore, accurate measurement of the engine rotary load is time intensive and costly. Hence, the condition monitoring (CM) of the transmitted torque and power of the tractor engine can be beneficial for control system applications. The above concerns were among the motivating elements to conduct this research.

The CM is the process of monitoring the condition parameter(s) in machinery (vibration, temperature, sound, etc.) in order to identify a significant change, which might be indicative of a developing fault. Moreover, the CM is a major element of predictive maintenance. Many publications on the CM to diagnose faults of mechanical systems and components, such as the metal lathe machine [4], rolling element [5], cutting tools [6,7], grinding process [8], mining equipment [9], pump-turbines [10], wind turbines [11], flexible rotor [12], centrifugal pump [13], reciprocating compressor [14], bearings [15–17], planetary gearboxes [18–22], gear transmission systems (a review) [23], helical gears [24], cylinder misfire [25], engine power disturbance [26] and engine valve leakage [27], have appeared in the literature, showing an attractive subject for scholarly speculation. In addition, the CM is used in control systems to assess the situation and make proper decisions. Monitoring the tractor engine load in agricultural operations with harsh working condition is one such CM application, which can assist the operator to regulate the engine load in accordance with the working conditions.

In automation control system applications, the CM of the

Abbreviations: PES, primary engine speed (rpm); IES, instantaneous engine speed (rpm); FCMF, fuel consumption mass flow ($g{\cdot}s^{-1}$); EGT, exhaust gas temperature (°C); MAEO, maximum exhaust opacity (m^{-1}); MEEO, mean exhaust opacity (m^{-1}); RPM, revolutions per minute (rpm); ANN, artificial neural network; RBF, radial basis function; CRD, completely randomized design; LSD, least significant difference; ANFIS, adaptive neuro fuzzy inference system; GP, grid partition; SC, subtractive clustering; FCM, fuzzy c-means; RMSE, root mean squared error; R^2, coefficient of determination; TSSE, total sum of squared error; EF, model efficiency; ANOVA, analysis of variance; MF, membership function; IC, internal combustion; SI, spark ignition; CI, compression ignition

* Corresponding author at: P.C. 9177948978, Mashhad, Iran.
E-mail address: abaspour@um.ac.ir (M.H. Abbaspour-Fard).

https://doi.org/10.1016/j.measurement.2018.02.050
Received 16 July 2017; Received in revised form 7 January 2018; Accepted 21 February 2018
Available online 23 February 2018

transmitted engine torque is unavoidable for control strategies [28]. Furthermore, manufacturers require to know the engine torque range in order to design the power train components (e.g., gearbox and crankshaft) and regulate the engine and gearbox for optimized performance and reduced emissions [29]. Several solutions are presented for driveline automation to manage the engine performance, all of which need accurate torque estimation [28]. For example, the engine torque is used in hybrid vehicle applications to assess the proportion of electric motor and thermal engine torque [30,31]. Furthermore, the engine torque is necessary for engine management [32,33]. As another example, an estimator for the transmitted clutch torque is used in the driveline to improve the clutch control performance during vehicle launch and gearshifts [34]. Zhao et al. [35] analyzed a dual clutch transmission (DCT) shifting process, wherein the torque transmitted by a twin clutch during the upshifting process was estimated by employing the unscented Kalman filter (UKF) algorithm. The experimental results demonstrated that the applied UKF torque estimation algorithm could adequately estimate the transmission torques of the two clutches in a real time manner.

Most of former researches on torque estimation have focused on internal combustion (IC) engine models. The inputs of these models typically consist of some engine measurements such as air [36] or fuel [37] mass flow, throttle position [38,39], fuel properties [40], spark advance [36,39], engine speed [36,37,39–41], and acoustic emission features [42]. Lee et al. [33] introduced two torque estimation techniques, namely “stochastic estimation technique” and “frequency analysis technique”, for an in-line, four-cylinder SI engine under a wide range of engine operating conditions (different engine speeds and loads). Franco et al. [43] presented a real-time engine brake torque estimation model, where the instantaneous engine speed served as the model input. Liu et al. [44] proposed a practical method to estimate the friction and torque load based on the characteristics of the instantaneous torque profile during an engine cycle. The work aimed to develop a practical solution for estimating the in-cylinder gas pressure from the crankshaft speed fluctuation. Lin et al. [45] employed instantaneous crank angular speed as a non-intrusive CM technique to estimate the load on a four-stroke, four-cylinder diesel engine in a laboratory condition. Aono et al. [46] developed an easier estimation method using finite impulse response (FIR) filter to derive the crankshaft rotational speed, which required less calculation load. The FIR filter for differentiation was designed based on the frequency domain characteristics between the crankshaft rotation speed and combustion torque. Numerous static and dynamic torque estimation methods were presented to monitor the engine torque [38,47]. In one study, four statistical methods were reviewed in a unified framework and compared for building the torque model: linear least squares, linear neural networks (NNs), non-linear NNs and support vector machines (SVMs). It was concluded that a non-linear model structure is essential for accurate torque estimation [29].

Soft computing methods are also appropriate for modeling diesel engines with highly nonlinear dynamic systems. These intelligent methods are used for identification, modeling, control and optimization purposes [48]. A variety of soft computing methods such as fuzzy [49–51], adaptive neuro fuzzy inference system (ANFIS) [52,53], SVM [54–56], local linear model tree (LoLiMoT) [57,58] and recurrent artificial neural network (RANN) [59,60] were used to model the performance parameters of IC engines. Among them, artificial neural networks (ANNs) were intensively employed for modeling and identification of IC engine parameters [4,54,61–67].

The ANN is a parallel computing system containing hardware and software [68]. It is widely used in various applications such as control systems, pattern recognition, robotics, manufacturing, optimization, forecasting, medicine, power systems, signal processing, and social and psychological sciences [69]. Moreover, it basically provides a non-deterministic mapping between sets of random input-output vectors. Learning directly from instances without attempting to estimate the statistical parameters is the main advantage of using ANNs [70]. With such capability, ANNs can be used for analyzing the engine behavior. The ANN is also a powerful tool for modeling engines based on input-output data [48]. Using the ANN to improve torque estimation of IC engines has become increasingly widespread [71]. Tosun et al. [40] used the ANN based on the back-propagation Levenberg-Marquardt (BPLM) training algorithm and linear regression (LR) modeling to predict engine torque and some other engine performance parameters of a diesel engine fueled with standard diesel and biodiesel-alcohol mixtures. Engine speed (rpm) and fuel properties (lower heating value, Cetane number and density) were applied as input parameters in order to predict the performance parameters. They mentioned that experimental determination of the performance and emission characteristics of an IC engine was complex, costly and time consuming. Therefore, they modeled the engine performance parameters using the ANN in order to eliminate these disadvantages and complexities. They used some parameters including exhaust temperature, fuel consumption and engine vibration as inputs and the models were presented for different fuel types, separately. The performance comparison of the LR and ANN showed that more accurate results can be obtained for the predicted parameters with the ANN technique. Noor et al. [37] utilized the ANN modeling based on a standard BPLM training algorithm to predict the output torque and some engine characteristics of a marine diesel engine, with various inputs such as engine speed and fuel flow rate. The results showed that the ANN model was more accurate than the mathematical model. The authors stated that the ANN was flexible and easy to use. Consequently, it can be preferred for many predictive data-mining applications. Moreover, the ANN is a robust, powerful and suitable technique for nonlinear and complex processes. Bietresato et al. [72] used ANNs to predict the instant torque and brake specific fuel consumption (BSFC) of farm tractor diesel engines with input parameters such as engine speed, exhaust gas (EG) temperature and motor oil temperature. ANNs were trained with EG and lubricant temperatures data through the error back-propagation algorithm.

Ge et al. [71] categorized the torque estimation models in two groups. In one category, the engine is modeled in detail according to the physical mechanism of engine, and then the engine torque is estimated using the detailed model [43,73,74]. In the other category, the complex nonlinear physical process of the detailed model is identified by using an ANN, resulting in a simplified model, and then the torque is estimated using the simplified model.

Togun and Baysec [39] presented a back-propagation (BP) network to predict the torque and BSFC of a 1400 cc, four-cylinder, four-stroke FIAT gasoline engine. The engine speed (in nine levels) as well as spark advance and throttle position (both in three levels) were used as inputs of the ANN models. The authors noted that the ANN model did not require detailed information of the system, and operated like a black box. Additionally, it was able to learn the relationship between the controlled/uncontrolled variables and input parameters by studying previously recorded data, similar to a nonlinear regression performance. As a prominent innovation, explicit mathematical formulations of torque and BSFC were presented based on the proposed ANN models.

Zweiri and Seneviratne [75] presented an ANN approach based on the BP algorithm to estimate the indicated torque of a single-cylinder diesel engine in terms of crankshaft angular velocity and displacement as input parameters. The authors mentioned that measuring these parameters did not need costly sensors; hence, the estimator may be practical in control or diagnostic strategies that require indicated torque, which is not simply measured and needs expensive sensor. Other prediction works related to the engine torque of IC engines based on the ANN approach were presented elsewhere [76–84].

Recently, many researchers have made comparative studies on different learning algorithms such as multilayer perception (MLP), SVM, radial basis function (RBF), and BP to predict the performance and emission characteristics of IC engines. Some of these studies are summarized in Table 1. As shown in the table, there are few comparative

Table 1
Some comparative studies of different learning algorithms for predicting the performance and emission characteristics of IC engines.

Researchers	Engine type (SI/CI[a])	Input parameters	Output parameters	Learning algorithms
Niu et al. [54]	CI	Rail pressure, injection timing, charge pressure, charge temperature	BSFC, soot, efficiency, max in-cylinder pressure, NO_x	Feed-forward BP + SVM
Shamshirband et al. [56]	CI	Fuel characteristics, load fraction, engine speed	Exergy and its components	SVM-RBF + SVM-wavelet transform + SVM-firefly algorithm + SVM-quantum particle swarm optimization + standard BP
Kumar et al. [69]	CI	Load percentage, compression ratio, blend percentage, injection timing, injection pressure	Brake thermal efficiency, brake specific energy consumption, exhaust gas temperature, CO, NO_x, UBHC, smoke	MLP + RBF
Rezaei et al. [86]	SI, CI	Butanol volume percentage, equivalence ratio	Indicated mean effective pressure (IMEP), net total heat released, maximum in-cylinder pressure, total hydrocarbon, CO, NO_x, indicated thermal efficiency	FF + RBF
Sharma et al. [87]	SI	Features extracted from vibration Signal (variance, kurtosis, minimum, mean, range, etc.)	Misfire detection of cylinders	J48 + best first tree + random forest tree + functional tree + linear model tree
Kökkülünk et al. [64]	CI	Engine speed, emulsified fuel percentage, operating load	CO, CO_2, NO, NO_x, HC, exhaust temperature	BP + RBF
Yap and Karri [88]	SI	Vehicle speed, air/fuel ratio, throttle position, tractive forces and power (in second stage)	Tractive forces and power (in first stage), tailpipe emission gases (CO, CO_2, HC, O_2 in second stage)	BP + optimization layer-by-layer (OLL) + RBF
Manjunatha et al. [89]	CI	Density, kinematic viscosity, blend, brake power, exhaust temperature	CO, CO_2, NO_x, HC, smoke	BP + RBF
Rohani et al. [70]	CI	Calendar age of tractor, tractor age as units of production, tractor age as cumulative hours of usage	Cumulative repair cost index, cumulative oil cost index, cumulative fuel cost index, cumulative repair and maintenance cost index	BP with Declining Learning-Rate Factor (BDLRF) + Basic BP
Wang et al. [90]	CI	Speed, max. pressure diff. and angle, angle difference of fixed pressure	NO_x	BP + RBF
Wu et al. [91]	SI	Features of sound emission signals	Six engine operating conditions (engine without fault, intake air leakage, one cylinder misfiring, two cylinders miss firing, fault in camshaft sensor and fault in engine coolant temperature sensor)	BP + RBF + probability ANN

[a] Spark-ignition/compression-ignition.

studies of engine torque estimation. The literature review revealed that the applications of RBF networks and ANFIS for modeling engine torque are rare. The prime benefit of using RBF feed-forward neural networks is less required training time, which is due to the simpler structure of these ANNs compared to MLP networks. Moreover, the RBF has comparatively low extrapolation errors and is generally more reliable [85]. Therefore, in the present study, the ability of the RBF neural network with various training algorithms and ANFIS was investigated to predict the CI engine torque under various working conditions, and their performances were compared. This was done with the aim of improving the accuracy of torque estimation.

In conclusion, the engine torque is one of the most important performance parameters of IC engines, which frequently needs to be estimated during operations. However its accurate measuring is laborious, time-consuming and costly. ITM285 is the most common tractor in Iran, which is widely used in agricultural operations. Accurate estimate of the output engine torque exerted by active agricultural implements through the tractor PTO shaft can be used for instantaneous system management during field operations.

This is an important and effective aspect of precision farming, which is developing in the current century. Hence, the main objective of this study was to develop engine torque estimation models in a wide range of engine operating conditions (load and speed) based on soft computing methods. The specific objectives were: 1 – to investigate and compare the effectiveness of the RBF neural network and ANFIS for engine torque estimation; 2 – to study the variation of the model performance with different model parameters; 3 – to select the most appropriate model for accurate prediction of the engine torque.

2. Materials and methods

2.1. Engine characteristics

Currently, ITM285 tractor is the most popular tractor in Iran. This tractor is adapted to different weather conditions in the country and hence, most of agricultural operations are performed by this model [92]. An ITM285 tractor was employed and the experiments were performed at the Department of Biosystems Engineering, College of Agriculture, Ferdowsi University of Mashhad, Iran. The detailed characteristics of the tractor's engine are shown in Table 2. Before commencing the experiments, all filters of the fuel and lubrication systems were renewed. Some preliminarily inspections were conducted to verify the instruments conditions (proper installations, appropriate transfer of data to PC, etc.) and ensure the proper status of the engine (checking the coolant and oil levels, adjusting the clearance of the intake and exhaust valves for each cylinder, etc.) before the main tests [93].

2.2. Experimental procedures

The experiments were conducted at 11 levels of primary engine speed (PES) including: 779, 921, 1063, 1204, 1346, 1488, 1629, 1771, 1818 (engine rated speed), 1913 and 2054 rpm (from 935 to 2465 rpm of the dynamometer speed by steps of 170 rpm). The tractor's PTO was coupled to a hydraulic dynamometer through a universal joint. At the beginning of each test, the engine speed was set and fixed at the desired level using the hand throttle lever of the tractor and the engine was sufficiently warmed up [94]. In other words, the engine hand throttle position was kept fixed while exerting the load. In each PES, the applied torque on the engine started from zero (no load) and continued to full load by increment of 10 N·m. As expected, the engine speed continuously decreased with increasing the applied torque. Hence, the engine speed at zero load and during the experiment (corresponding to the applied torque) was named PES and instantaneous engine speed (IES), respectively. The overall view of the test setup is shown in Fig. 1. The measured parameters included fuel consumption mass flow (FCMF), exhaust gas temperature (EGT), IES, maximum exhaust opacity (MAEO) and mean exhaust opacity (MEEO). The experiments were carried out at ambient temperature range of 23 ± 7 °C [95].

Table 2
Characteristics of the tractor's engine.

Engine type	Perkins, four-cylinder, four-stroke, CI
Model year (MY)	2005
Cylinder bore	101 mm
Cylinder stroke	127 mm
Compression ratio	16:1
Fuel	Diesel fuel
Fuel pump	In-line injection pump
Combustion system	Direct injection
Maximum power	75 hp @ engine speed of 2000 rpm
PTO RPM	540 rpm @ engine speed of 1818 rpm

Fig. 1. The overall view of the test setup.

2.3. Measuring parameters

A hydraulic water-flow dynamometer (PLINT, England) with maximum loading capacity of 325 N·m, resolution of 0.1 N·m and measuring range of 0–325 N·m was used to exert rotational load on the engine via the PTO shaft (Fig. 1). The instrumentations for measuring the parameters and the schematic of the test bed are shown in Figs. 2 and 3, respectively. Data recording was performed after achieving stability in values of the instrumentations at each new torque or speed point [93]. To measure the torque applied on the engine by the dynamometer, it was equipped with a load cell with capacity of 100 kg. The load cell output was sent to a PC and then converted to torque unit by multiplying with torque arm (0.365 m). Prior to starting the experiments, the dynamometer was statically calibrated using the existing standard weights (two weights corresponding to 50 N·m and two weights to 75 N·m). Moreover, the rotational measuring component of the dynamometer was calibrated using an optical tachometer. The readings of the dynamometer for the RPM (resolution of 1 rpm, measuring range of 0–3000 rpm, accuracy of 0.1%) and torque were received by an electronic interface circuit, digitally sent to the PC and then, displayed on a monitor. The conversion ratio of the engine speed to dynamometer speed was 1:1.2. In other words, the engine speed was calculated by dividing the dynamometer speed to 1.2. For precise adjustment of a PES at an intended level, the tractor's hand throttle was disconnected from the injection pump and replaced with a suitable scaled screw on the control rack lever of the injection pump.

Fuel consumption (by mass) was accurately determined by means of a digital scale through weighing a temporary small fuel supply container (instead of the tractor's main fuel tank). The volumetric measurement of fuel consumption is much easier than the mass

Fig. 2. The instrumentations for the parameters measurements: 1 – Digital scale to measure fuel consumption, 2 – Diesel emission tester, 3 – Temperature monitor and sensor, 4 – Emission probe and 5 – Load cell.

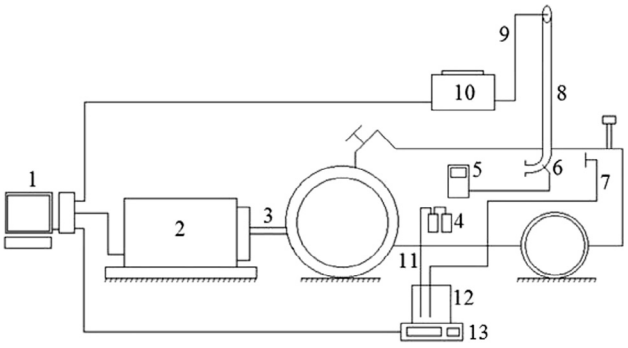

Fig. 3. Schematic of the test bed: 1 – Data acquisition system, 2 – Dynamometer, 3 – Universal joint, 4 – Primary fuel filters, 5 – Temperature monitor, 6 – Temperature sensor, 7 – Fuel return pipe, 8 – Tractor exhaust, 9 – Emission measurement probe, 10 – Diesel emission tester, 11 – Fuel inlet pipe, 12 – Fuel container and 13 – Digital scale.

measurement; however, temperature corrections must be applied [93]. When consumption is measured by volume, the fuel density at 15 °C should be multiplied by the fuel temperature, at which the measurement is made [95]. Hence, fuel density variations with temperature must be considered. A digital scale (Japan, A&D Co., GF-6100 model, repeatability/Std. Dev. of 0.01 g, linearity of ± 0.03 g, measuring range of 0–6.1 kg, resolution of ± 0.01 g) was used to measure FCMF of the engine (Fig. 2). The tractor's fuel tank was disconnected from the fuel system and instead, a small fuel container was used and carefully put on the scale. The fuel flow from the container was conveyed to primary fuel filters through a plastic pipe and another pipe was used to return the surplus fuel from injectors to the container (Fig. 3). The weight of the container on the scale was recorded with the sampling rate of five samples per second. Afterwards, the scatter plot of the recorded values was drawn by Excel software and then, the trend line of the plot was fitted. The FCMF was determined in gram per second, which corresponded to the slop of the trend line.

A diesel emission tester (Germany, MAHA Co., MDO2-LON model, measuring range of 0–9.99 m^{-1}, and resolution of 0.01 m^{-1}) was used to measure the exhaust opacity (Fig. 2). Before starting the experiments, the device was calibrated by the authorized company (Iran, Tavan Sazan Co.). The device measured and recorded the exhaust opacity in m^{-1} and displayed the variations of the MAEO at the end of each test run.

A K-type temperature sensor (thermocouple) capable of measuring temperature up to 700 °C (resolution of 1 °C, accuracy of ± 2 °C) [96] was installed on the exhaust elbow [97]. Moreover, a temperature monitor (Lutron Co., TM-902C model, capable of monitoring temperature from −50 to 1300 °C, resolution of 1 °C) was used (Fig. 2). The accuracy of the temperature sensor was examined by measuring the temperatures of the saturated mixture of water and ice (0 °C) and boiling water (99.62 °C) at atmospheric pressure of 100 kPa [98]. The exhaust elbow was drilled to install the temperature sensor on the engine [97] and a hexagon nut was welded on the drilled hole. The sensor completely entered into the elbow by tightening the sensor base to the nut (Fig. 2). The exhaust elbow was selected to install the temperature sensor for two reasons: 1 – all exhaust gases of the cylinders passed through this component, and 2 – this component was the nearest place to the exhaust manifold and hence, minimum reduction of exhaust gas temperature occurred. Precisely speaking, the midpoint of the elbow curvature was considered as the installation location of the sensor, where the exhaust gases passed tangentially to the internal wall and hence, better affected the temperature sensor (Fig. 3).

2.4. Data analysis

2.4.1. Radial basis function (RBF) model

In the present study, the RBF neural network model was employed to estimate the engine output torque. The RBF is a kind of learning algorithm method of ANNs, which offers faster prediction than a conventional simulation program or mathematical technique [89]. An RBF-based ANN structure includes three layers named input, hidden, and output layers [64]. The hidden layer consists of many RBF neurons and its nodes are calculated from the Euclidean distance between the center and network input vectors [99]. The RBF neural network offers more

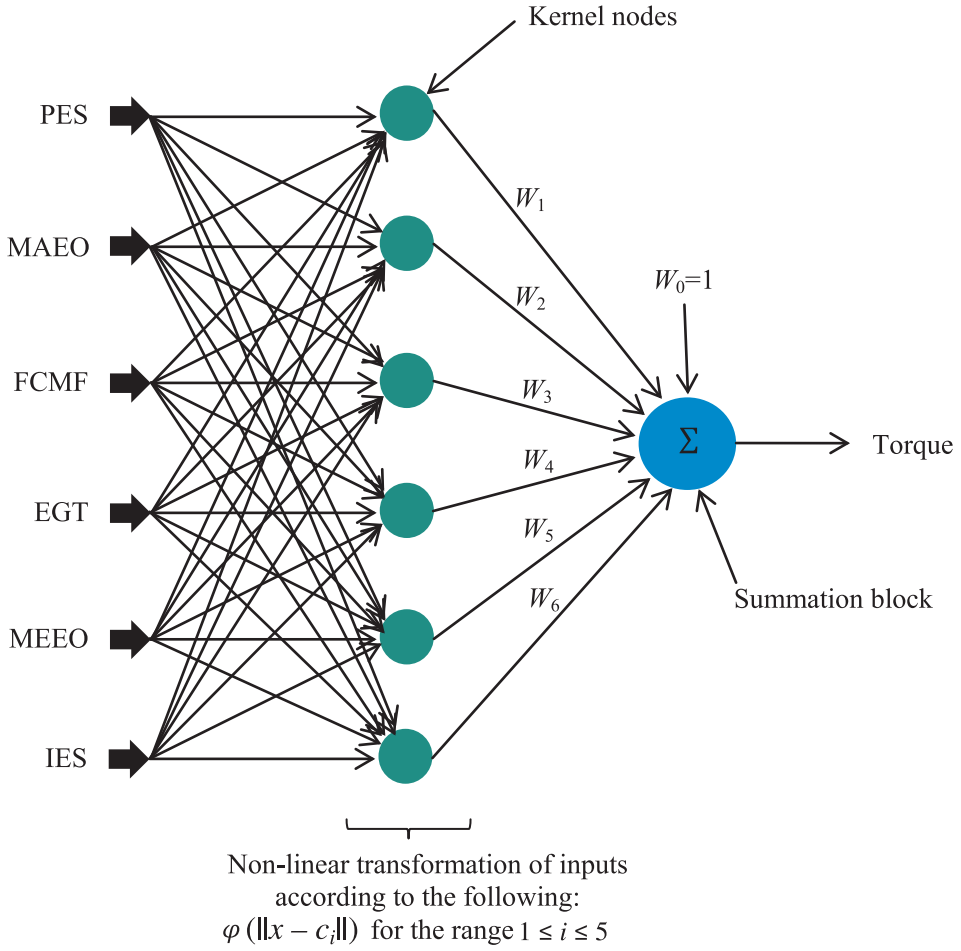

Fig. 4. The RBF feed-forward neural network.

effective methods to train and organize its structure and does not have the problem of trapping into the local minimum [91]. It is one of the variants of feed-forward ANN types. Such ANNs are applied to execute mapping functions of the form f: $\mathscr{R}^n \rightarrow \mathscr{R}$. sed on the following equation:

$$f(x) = W_0 + \sum_{i=0}^{m} W_i \varphi(\|x - c_i\|) \tag{1}$$

where $x \in \mathscr{R}^n$. presents the input vector, $\varphi(.)$. a non-linear transformation function, $\|.\|$. presents the Euclidean distance, W_i. ving a range of $1 \leqslant i \leqslant m$. presents the weights, $c_i \in \mathscr{R}^n$. ving a range of $1 \leqslant i \leqslant m$. notes the kernel nodes or centers, and m. presents the number of kernel nodes. A radial basis function network based on Eq. (1), which is adopted for the inputs and output of this study, is shown in Fig. 4 [85].

Thirteen training algorithms including Bayesian regularization (Trainbr), BFGS quasi-Newton back-propagation (Trainbfg), Powell-Beale conjugate gradient back-propagation (Traincgb), scaled conjugate gradient back-propagation (Trainscg), Fletcher-Powell conjugate gradient backpropagation (Traincgf), one step secant back-propagation (Trainoss), Polak-Ribiere conjugate gradient back-propagation (Traincgp), Levenberg-Marquardt back-propagation (Trainlm), resilient back-propagation (Trainrp), gradient descent w/momentum and adaptive lr back-propagation (Traingdx), gradient descent with adaptive lr back-propagation (Traingda), gradient descent with momentum back-propagation (Traingdm) and gradient descent back-propagation (Traingd) were used to examine their effectiveness in training the RBF neural network. Kumar et al. [69] used four different training algorithms (Trainrp, Traingdx, Trainscg and Trainlm) for training the network. The training algorithms were compared together using the combination of three statistical methods namely: k-fold cross validation [70], completely randomized design (CRD) and least significant difference (LSD).

2.4.2. Adaptive neuro fuzzy inference system (ANFIS) model

In addition to the RBF neural network, the ANFIS model was used as an alternative method for estimating the engine torque. The ANFIS model can extract relationships between the inputs and output (torque) based on some fuzzy rules. In order to reduce the computations of the fuzzy model, some of the independent variables were selected and used as inputs of the ANFIS model, based on the results obtained from sensitivity analysis of the RBF model. Three methods, namely comprising grid partition (GP), subtractive clustering (SC) and fuzzy c-means (FCM) clustering, were used to construct the fuzzy inference system (FIS) structure. For a better comparison between the ANFIS and RBF models, the same datasets of the RBF model were also used for the ANFIS model.

2.5. Evaluation of models' performance

Some important and common criteria including root mean squared error (RMSE), coefficient of determination (R^2), total sum of squared error (TSSE) and model efficiency (EF) were used to evaluate the models' performance. They are defined as follows [70]:

$$\text{RMSE} = \sqrt{\sum_{i=1}^{n} (dv - pv)^2 / n} \tag{2}$$

$$R^2 = \frac{(\sum_{i=1}^{n} (dv - \overline{dv})(pv - \overline{pv}))^2}{\sum_{i=1}^{n} (dv - \overline{dv})^2 \sum_{i=1}^{n} (pv - \overline{pv})^2} \tag{3}$$

$$\mathrm{TSSE} = \sum_{i=1}^{n} (dv - pv)^2 \tag{4}$$

$$\mathrm{EF} = 1 - \frac{\sum_{i=1}^{n} (dv - pv)^2}{\sum_{i=1}^{n} (dv - \overline{pv})^2} \tag{5}$$

where dv is the actual (desired) output; pv is the predicted (fitted) output produced by the model; and $\overline{d}$ and $\overline{p}$ are the average of the desired and predicted output, respectively. A model with the lowest RMSE and TSSE and the highest EF and R^2 is considered to be the best.

The mean, variance, kurtosis and skewness of the actual and predicted datasets were statistically compared to evaluate the RBF model performance through the training, test and total phases. Some statistical tests such as paired *t*-test, F-test and Kolmogorov–Smirnov test were used to compare the mean, variance and statistical distribution of the two datasets.

3. Results and discussion

Two parameters, namely spread parameter and number of neurons in the hidden layer, affected the performance prediction of the RBF neural network. The variations of the RMSE and EF for all the data (train and test) against the spread parameter are shown in Fig. 5(a). The number of neurons in the hidden layer was assumed to be constant and equal to 10. As it was seen, with increase in the spread parameter, the RMSE and EF had downward and upward trends, respectively. Our investigation showed that the trend of the spread parameter variations changed for the spread parameter of greater than 0.8. Fig. 5(b) shows the effect of the number of neurons (hidden size) in the hidden layer on the performance of the RBF neural network. As shown in this figure, the RMSE had downward trend with increase in the number of neurons. However, the number of neurons had no noticeable effect on the EF. Hence, it can be concluded that the EF was only affected by the optimum value of the spread parameter. On the basis of Fig. 5, it can be concluded that having 10 neurons was the best state for the network. Increasing the number of neurons more than 10 could lower the RMSE; however, this reduction was negligible, considering training and computing times.

In the next step, the thirteen selected training algorithms previously mentioned were evaluated for engine torque predictions. The combination of the CRD and k-fold cross validation methods was used to evaluate the training algorithms. The analysis of variance (ANOVA) of the CRD is shown in Table 3 considering the RMSE, TSSE, EF and R^2 criteria. Each training algorithm was trained using 20 different datasets obtained from 5-fold cross validation with four replications. Consequently, the total degree of freedom (df) of the CRD was 259 according to the 13 treatments (the training algorithms) and 20 replications (the datasets). The p-values obtained from F statistic demonstrated that the training algorithms had significant differences at the one percent probability level based on the four performance criteria.

Means comparison of the RMSE, TSSE, EF and R^2 criteria was performed using the LSD method. The means comparison result of the performance criteria of the 13 RBF's training algorithms is shown in Table 4. It was observed that the RMSE and TSSE criteria demonstrated the differences of the training algorithms better than the R^2 and EF criteria. This was because most of the training algorithms except Traingdm had not significant differences with each other based on the R^2 and EF criteria. Moreover, the RMSE represented the differences of the algorithms better than the TSSE, because it classified the algorithms in various classes. Hence, the selection of the algorithms was optimized based on the smaller value of the RMSE. The results showed that the Traindm algorithm, in comparison with the others, had the worst performance with significant difference at the one percent probability level. The algorithms can be arranged based on the RMSE in ascending order as follows: Trainbr, Trainbfg, Traincgb, Trainscg, Traincgf, Trainoss, Traincgp, Trainlm, Trainrp, Traingdx, Traingda, Traingdm and Traingda. Although the Trainlm algorithm was used to train the RBF in most studies [69,86], the results of the present study showed that this algorithm was ranked eighth among the 13 algorithms and the Trainbr algorithm was selected as the best. It should be noted that although the Trainbr algorithm had no significant difference with the Trainbfg algorithm, its RMSE and TSSE values were 15 and 40 percent lower than those of the Trainbfg algorithm, respectively. The performance of the RBF neural network might be varied with different data sets. Hence, among the 20 different data sets from the 5-fold cross validation, the data set with the ability to lower the errors of the training phase, assign good generalization to the RBF network and prevent overfitting was selected as the best training and test data set.

The result of the RBF performance evaluation for estimating the ITM285 tractor engine torque is shown in Table 5. As seen, the values of the mean, variance, kurtosis and skewness of the actual and predicted data sets in the training, test and total phases were displayed to evaluate the RBF model performance. However, as shown in this table, the differences between the values were not considerable. Nevertheless, the values were statistically compared together. Statistical tests, namely paired *t*-test, F-test and Kolmogorov–Smirnov test, were used to compare the mean, variance and statistical distribution of the actual and predicted data sets, respectively. The p-values obtained from all the tests were greater than 0.05. Consequently, no statistically significant

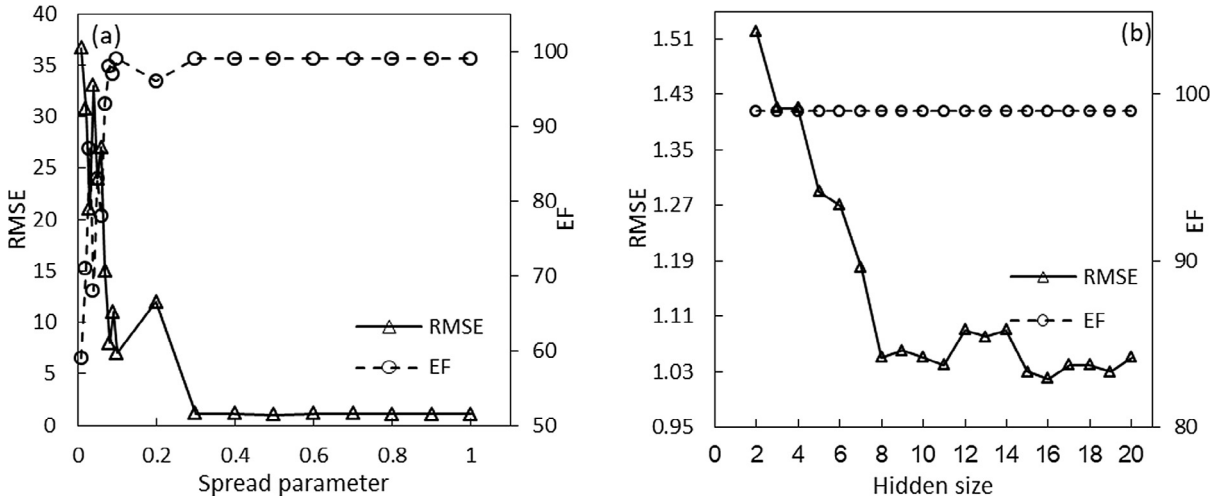

Fig. 5. Variations of the RMSE and EF versus the spread parameter and hidden size.

Table 3
ANOVA of the performance criteria of the RBF network for different training algorithms using CRD.

Source	DF	RMSE		TSSE		EF		R^2	
		SS	F-value	SS	F-value	SS	F-value	SS	F-value
Treatments[a]	12	4174.24	2654.83**	50.37×10^{-9}	1019.6**	0.1138	1019.96**	0.0216	321.56**
Errors	247	32.36		1.02×10^{-9}		0.0023		0.0014	
Total	259	4206.60		51.39×10^{-9}		0.1161		0.0230	

[a] The training algorithms.
** Significant at the 1% level.

Table 4
Means comparison of the performance criteria of the RBF network for various training algorithms.

Training algorithms	RMSE	TSSE	EF	R^2
Trainlm	1.14 ± 0.23^{cd}	275.20 ± 152.31^{a}	0.99 ± 0.00^{a}	0.99 ± 0.00^{a}
Trainbr	*0.70 ± 0.00^{a}*	*100.68 ± 0.33^{a}*	*0.99 ± 0.00^{a}*	*0.99 ± 0.00^{a}*
Trainscg	0.99 ± 0.08^{bcd}	199.56 ± 39.94^{a}	0.99 ± 0.00^{a}	0.99 ± 0.00^{a}
Trainrp	1.17 ± 0.06^{d}	281.62 ± 32.62^{a}	0.99 ± 0.00^{a}	0.99 ± 0.00^{a}
Traingdx	1.67 ± 0.45^{e}	607.14 ± 680.50^{a}	0.99 ± 0.00^{a}	0.99 ± 0.00^{a}
Traingdm	3.63 ± 0.62^{g}	2753.68 ± 956.54^{b}	0.99 ± 0.00^{b}	0.99 ± 0.00^{b}
Traingda	2.22 ± 0.82^{f}	1137.91 ± 1921.34^{a}	0.99 ± 0.00^{a}	0.99 ± 0.00^{a}
Traingd	15.53 ± 1.65^{h}	$49301.02 \pm 10256.70^{c}$	0.92 ± 0.01^{c}	0.96 ± 0.01^{a}
Trainbfg	0.83 ± 0.04^{ab}	140.20 ± 16.24^{a}	0.99 ± 0.00^{a}	0.99 ± 0.00^{a}
Traincgb	0.94 ± 0.07^{bc}	182.01 ± 27.69^{a}	0.99 ± 0.00^{a}	0.99 ± 0.00^{a}
Traincgf	1.00 ± 0.06^{bcd}	203.41 ± 26.20^{a}	0.99 ± 0.00^{a}	0.99 ± 0.00^{a}
Traincgp	1.02 ± 0.05^{bcd}	213.56 ± 24.60^{a}	0.99 ± 0.00^{a}	0.99 ± 0.00^{a}
Trainoss	1.01 ± 0.04^{bcd}	209.55 ± 19.99^{a}	0.99 ± 0.00^{a}	0.99 ± 0.00^{a}

Means with the same letters are not significantly different.
The item with italics shows the best training algorithm.

difference was observed between the actual and predicted data sets. Furthermore, the values of the RMSE and EF in the training and test phases were approximately equal to 0.58. This shows that the RBF network has good generalization.

The agreement between the actual and predicted values during the training and test phases is shown in Fig. 6. As can be seen, the points were scattered around the line of 45 deg. On the other hand, the coefficient of determination (R^2) of the regression line between the actual and predicted values was 0.99 in both the training and test phases. Moreover, the slope and intercept of the line were close to one and zero, respectively. Considering this result, it can be concluded that there is a very good agreement between the actual and predicted values in both the training and test phases. Moreover, the agreement between the actual and predicted values of the torque for all the samples during the training and test phases is shown in Fig. 7. Zweiri and Seneviratne [75] concluded that the average deviation between the measured and estimated torque was not excessive and that the ANN-based nonlinear torque estimator demonstrated a good agreement and high potential.

Sensitivity analysis was carried out to investigate the effect of the six studied variables for estimating the engine torque. The sensitivity analysis results of the RBF model after excluding the input variables in the training, test and total phases are shown in Table 6. As can be seen, the exclusion of four independent variables (PES, FCMF, EGT and IES) from the inputs of the RBF neural network increased the error (TSSE and RMSE) during the training, test and total phases. It is implied that for a better performance, this set of input variables of the network should be used; while the exclusion of the two remaining variables (MAEO and MEEO) can enhance the network performance. Consequently, the set of input variables including PES, FCMF, EGT and IES was used as the best combination. It can be concluded that using the aforementioned variables and removing the MAEO and MEEO can improve the network prediction performance. For instance, with this set of measurements, the RMSE approximately decreased by 15 percent in the training, test and total phases. Moreover, the unnecessary measurement of the opacity parameter decreased estimation costs due to removal of the opacity sensor from the measuring system of the tractor engine torque. Franco et al. [43] mentioned that some variables such as pressure and temperature of intake and exhaust manifolds, engine speed, fuel quantity, and engine geometry had a significant impact on engine brake torque. In other researches, lubricant temperature was inappropriate (very low and diversified R^2) to model engine torque and BSFC using ANNs; while, EGT proved to be a suitable indirect estimator

Table 5
The RBF network performance for estimating the engine torque.

	Train phase			Test phase			Total		
	Actual	Predicted	p-value	Actual	Predicted	p-value	Actual	Predicted	p-value
Average	86.23	86.23	0.99	98.33	98.33	0.99	90.15	90.15	0.99
Variance	3301.88	3300.81	0.99	2931.61	2930.07	0.99	3309.93	3309.06	0.99
Kurtosis	1.84	1.84	0.99	2.28	2.29	0.99	1.89	1.89	0.99
Skewness	0.17	0.17		0.35	0.35		0.15	0.15	
RMSE	0.59			0.58			0.58		
TSSE	56.39			13.22			69.70		
EF	0.99			0.99			0.99		

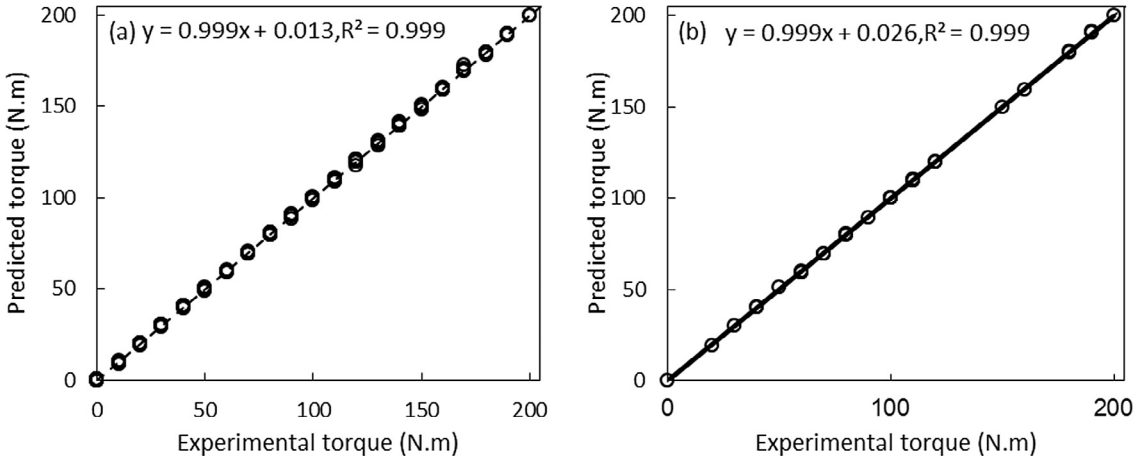

Fig. 6. Scatter plot of the actual and predicted data sets in the (a) training phase and (b) test phase.

(R^2 > 0.993) [72].

3.1. Adaptive neuro fuzzy inference system (ANFIS) model

As mentioned, the ANFIS model was used as an alternative tool to estimate the engine torque. Based on the sensitivity analysis results of the RBF model, and to reduce the computations of the fuzzy model, the independent variables including PES, FCMF, EGT and IES were used as the ANFIS model inputs. The ANFIS model can extract the relationships between the inputs and torque (the output) based on fuzzy rules, which dominate the problem. As previously mentioned, the GP, SC and FCM methods were used to construct the FIS structure. To evaluate each method, individual parameters and their different combinations were examined and results are shown in Tables 7–9. Various membership functions (MFs) were evaluated for the GP method and the results showed that Gaussian was the best one. Using various MF numbers showed that the MF number of all the three methods provided the best result for each input. It should be mentioned that increasing the MF number did not considerably improve the ANFIS performance and only increased the training time of the model. Between linear and constant functions as the output MF, the latter provided a better result. The best condition was obtained from ANFIS-GP4.

The optimum values of the SC model parameters including the influence radius, squash factor and MF number of the input and output were obtained through trial and error. In all the cases, the values of the accepted ratio and rejected ratio parameters were considered 0.5 and

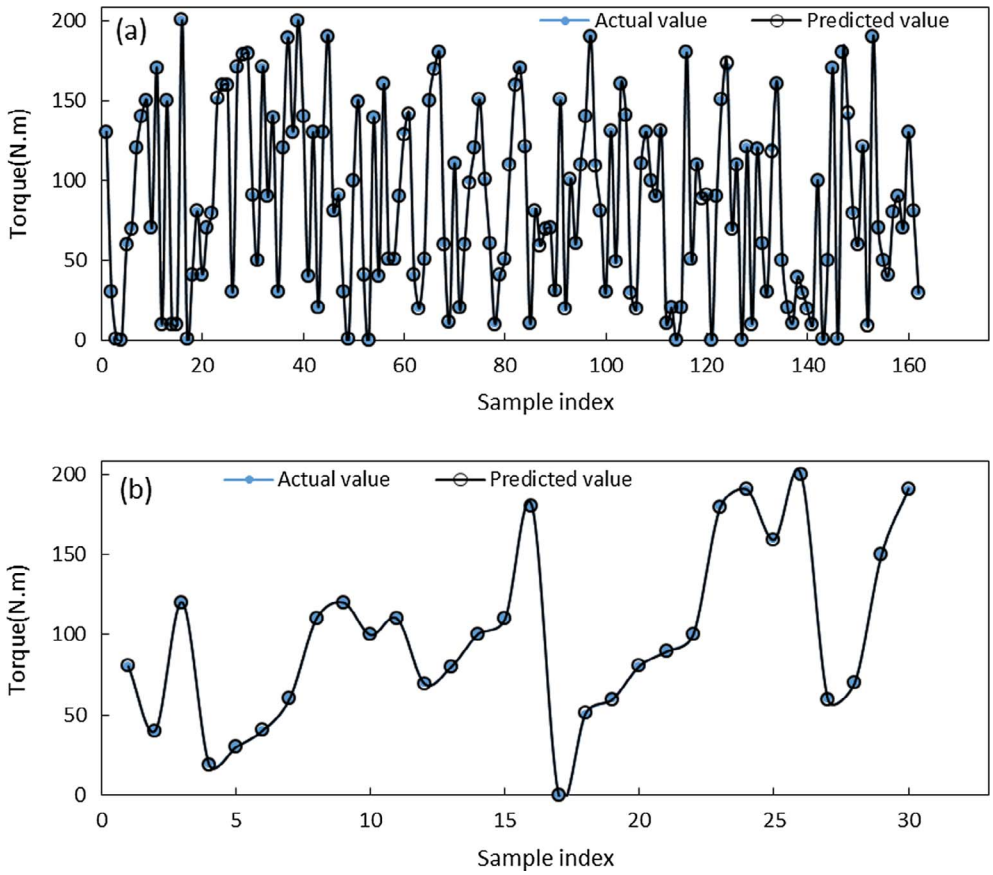

Fig. 7. The actual and predicted values of the torque in the (a) training phase and (b) test phase using the RBF.

Table 6
The sensitivity analysis results of the RBF model.

Model	Input set	Train phase			Test phase			Total		
		RMSE	TSSE	EF	RMSE	TSSE	EF	RMSE	TSSE	EF
All	All	0.59	56.39	0.99	0.58	13.32	0.99	0.58	69.70	0.99
Sensitivity analysis	All exclude PES	0.69	77.55	0.99	0.68	19.02	0.99	0.69	96.57	0.99
	All exclude MAEO	**0.58**	**55.94**	**0.99**	**0.57**	**13.61**	**0.99**	**0.58**	**69.55**	**0.99**
	All exclude FCMF	0.72	85.79	0.99	0.72	21.22	0.99	0.72	107.01	0.99
	All exclude EGT	0.86	121.41	0.99	0.85	30.25	0.99	0.86	151.66	0.99
	All exclude MEEO	**0.59**	**57.28**	**0.99**	**0.58**	**14.22**	**0.99**	**0.59**	**71.53**	**0.99**
	All exclude IES	0.74	90.51	0.99	0.74	22.78	0.99	0.74	113.29	0.99
Proper selected input set	PES, FCMF, EGT, IES	0.50	40.90	0.99	0.51	10.60	0.99	0.50	51.49	0.99

Table 7
The performance and some characteristics of the ANFIS-GP model.

Model name	Number of input MF	Type of input MF	Type of output MF	Number of output MF	Number of rule	Epochs	RMSE	TSSE	EF
GP1	[2 2 3 3]	gaussMF	Constant	[24]	24	90	0.94	179.96	0.99
GP2	[2 3 3 2]	gaussMF	Constant	[24]	24	190	1.42	408.24	0.99
GP3	[3 3 2 2]	gaussMF	Constant	[24]	24	180	1.17	277.73	0.99
GP4	[3 3 3 3]	gaussMF	Constant	[81]	81	2000	0.70	99	0.99

Table 8
The performance and some characteristics of the ANFIS-SC model.

Model name	Influence Radius	Squash Factor	Number of input MF	Number of output MF	Number of rule	Epochs	RMSE	TSSE	EF
SC1	0.13	1.5	[3 3 3 3]	[3]	3	1800	1.23	303	0.99
SC2	0.15	1.5	[5 5 5 5]	[5]	5	4500	0.97	188	0.99
SC3	0.12	1.2	[7 7 7 7]	[7]	7	1100	0.83	138	0.99
SC4	0.15	1.5	[9 9 9 9]	[9]	9	2500	0.61	76.04	0.99

Table 9
The performance and some characteristics of the ANFIS-FCM model.

Model name	Number of cluster	Number of input MF	Number of output MF	Number of rule	Epochs	RMSE	TSSE	EF
FCM1	3	[3 3 3 3]	[3]	3	500	1.17	276	0.99
FCM2	5	[5 5 5 5]	[5]	5	350	0.84	143	0.99
FCM3	7	[7 7 7 7]	[7]	7	550	0.74	108	0.99
FCM4	9	[9 9 9 9]	[9]	9	450	0.60	73	0.99

0.15, respectively. In addition, the MF types of the input and output in all the cases were selected Gaussian and linear, respectively. The best prediction performance of the ANFIS-SC model with nine MFs for each input was obtained by the values of 0.15 and 1.5 for the influence radius and squash factor, respectively (Table 8). The results of this model also showed that the prediction performance of the model was improved by increasing the MF number. The optimum MF number of each input and output was nine and any further increase did not considerably improve the performance of the ANFIS-SC model.

The other method for constructing the FIS was the FCM. This method determines the MFs number of inputs and output. In this method, Gaussian and linear were also used as the input and output MF, respectively. As can be seen (Table 9), the number of rules and inputs and output MF were the same as the clusters number. The results showed that the prediction performance of the model was improved by increase in the clusters number. The clusters number of nine was selected as the optimum number. With increase in this number, computations of the model increased and the prediction performance was not considerably improved.

3.2. Comparison of radial basis function (RBF) and adaptive neuro fuzzy inference system (ANFIS)

The results of the RBF neural network and ANFIS performance with the three methods of GP, SC and FCM in the training, test and total phases are shown in Table 10. In these models, four independent variables including PES, FCMF, EGT and IES were considered as model inputs. A detailed profile of estimation errors between the actual and predicted values [55] of the engine output torque for the models on the training and test datasets is shown in Fig. 8. It is evident that the RBF model exhibited better approximation accuracy, especially during the test phase. As the results show, the average efficiency (EF) of all the

Table 10
Comparison of the RBF and various ANFIS models.

Model	Train phase			Test phase			Total		
	RMSE	TSSE	EF	RMSE	TSSE	EF	RMSE	TSSE	EF
RBF	0.50	40.90	0.99	0.51	10.60	0.99	0.50	51.49	0.99
ANFIS_GP4	0.56	50.33	0.99	1.10	48.73	0.99	0.70	99	0.99
ANFIS-SC4	0.45	33.17	0.99	1.04	42.87	0.99	0.61	76.04	0.99
ANFIS-FCM4	0.46	34.71	0.99	0.98	38.30	0.99	0.60	73	0.99

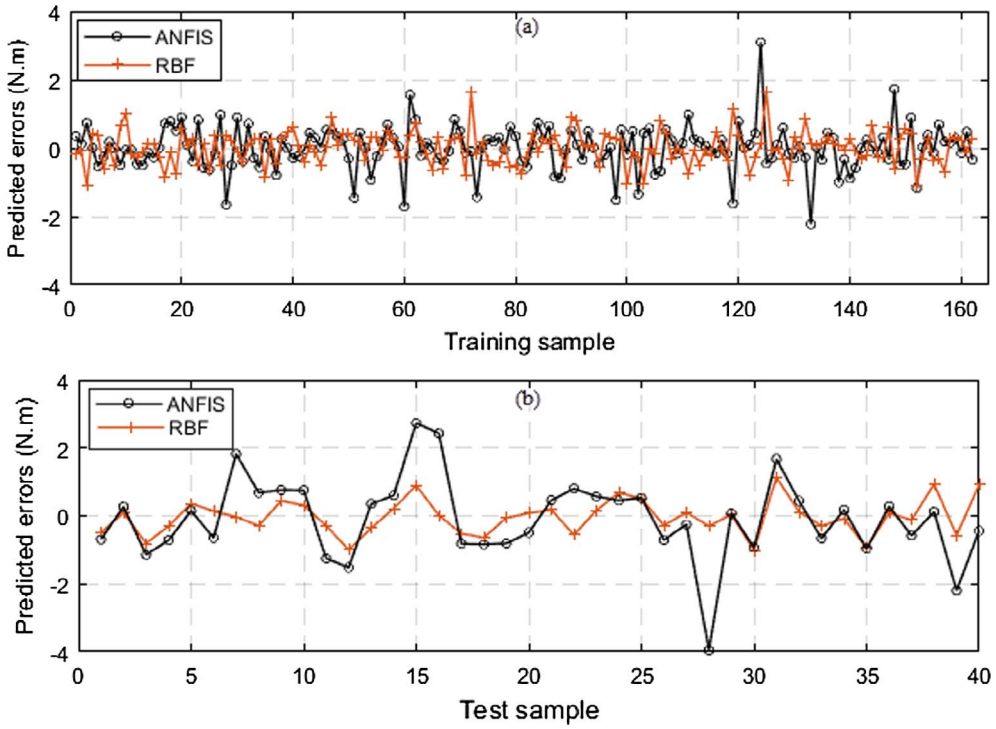

Fig. 8. Prediction errors of the engine output torque for the models on the (a) training dataset and (b) test dataset.

models in all the phases was 0.99. However, considering the RMSE and TSSE, they can be ranked in a descending order as: ANFIS-GP4, ANFIS-SC4, ANFIS-FCM4 and RBF. It should be noted that although the RMSE and TSSE of the ANFIS-SC4 and ANFIS-FCM4 models were greater than the RBF model, the reverse result was obtained in the training phase. This means that although the ANFIS model had better learning capability than the RBF model, over-fitting occurred because the RMSE and TSSE of the ANFIS models in the test phase were greater than the RBF. Moreover, the RMSE of the RBF model in both the training and test phases was approximately equal to 0.5.

4. Conclusion

With the aim of engine torque estimation, some models were developed based on ANNs and the ANFIS, using some easy to measure working characteristics of ITM285 tractor including PES, IES, FCMF, EGT, MEEO and MAEO. According to the outcome of this research, the engine torque can be estimated using some low-cost sensors instead of expensive devices and equipment (e.g., dynamometer). Sensitivity analysis demonstrated that two independent inputs of the MAEO and MEEO can be eliminated from the engine torque estimation procedure and better prediction performance can be gained by use of the four inputs of PES, FCMF, EGT and IES.

Moreover, the proposed model had high accuracy and simplicity in predicting the engine output torque. Hence, it can be used as a soft surrogate sensor. At the end of the training phase, the optimum weights of the RBF were obtained, which can be used as a final model in a micro switch for torque estimation. It should be noted that the micro switch receives data via the aforementioned sensors. This data was used as inputs for the model, while the output of the model was the engine torque applied for control systems.

The results of this research also revealed that models based on soft computations are able to estimate the torque of the ITM285 tractor's engine using data obtained from inexpensive and accessible sensors. Hence, the proposed models can be substituted with the conventional, highly expensive methods that use dynamometers.

Acknowledgment

The work presented in this paper is funded by the Research Deputy of Ferdowsi University of Mashhad, Iran. It is part of a PhD thesis fulfilled at the Department of Biosystems Engineering. Their contributions are warmly acknowledged.

References

[1] M.R. Seifi, S.R. Hassan-Beygi, B. Ghobadian, U. Desideri, M. Antonelli, Experimental investigation of a diesel engine power, torque and noise emission using water–diesel emulsions, Fuel 166 (2016) 392–399, http://dx.doi.org/10.1016/j.fuel.2015.10.122.
[2] E.Y. Kim, A.C. Tan, B.-S. Yang, Acoustic emission for diesel engine monitoring: a review and preliminary analysis, in: Engineering Asset Management and Infrastructure Sustainability, Springer, 2012, pp. 489–499. https://doi.org/10.1007/978-0-85729-493-7_37.
[3] N. Jones, Y.H. Li, A review of condition monitoring and fault diagnosis for diesel engines, Lubr. Sci. 6 (2000) 267–291, http://dx.doi.org/10.1002/tt.3020060305.
[4] A.B. Garg, P. Diwan, M. Saxena, Artificial neural networks for internal combustion engine performance and emission analysis, Int. J. Comput. Appl. 87 (2014).
[5] P. Nguyen, M. Kang, J.-M. Kim, B.-H. Ahn, J.-M. Ha, B.-K. Choi, Robust condition monitoring of rolling element bearings using de-noising and envelope analysis with signal decomposition techniques, Expert Syst. Appl. 42 (2015) 9024–9032, http://dx.doi.org/10.1016/j.eswa.2015.07.064.
[6] M. Bhuiyan, I. Choudhury, M. Dahari, Y. Nukman, S. Dawal, Application of acoustic emission sensor to investigate the frequency of tool wear and plastic deformation in tool condition monitoring, Measurement 92 (2016) 208–217, http://dx.doi.org/10.1016/j.measurement.2016.06.006.
[7] M. Elangovan, S.B. Devasenapati, N. Sakthivel, K. Ramachandran, Evaluation of expert system for condition monitoring of a single point cutting tool using principle component analysis and decision tree algorithm, Expert Syst. Appl. 38 (2011) 4450–4459, http://dx.doi.org/10.1016/j.eswa.2010.09.116.
[8] I. Mukherjee, S. Routroy, Comparing the performance of neural networks developed by using Levenberg–Marquardt and Quasi-Newton with the gradient descent algorithm for modelling a multiple response grinding process, Expert Syst. Appl. 39 (2012) 2397–2407, http://dx.doi.org/10.1016/j.eswa.2011.08.087.
[9] D.V. Petrović, M. Tanasijević, V. Milić, N. Lilić, S. Stojadinović, I. Svrkota, Risk assessment model of mining equipment failure based on fuzzy logic, Expert Syst. Appl. 41 (2014) 8157–8164, http://dx.doi.org/10.1016/j.eswa.2014.06.042.
[10] E. Egusquiza, C. Valero, D. Valentin, A. Presas, C.G. Rodriguez, Condition monitoring of pump-turbines. New challenges, Measurement 67 (2015) 151–163, http://dx.doi.org/10.1016/j.measurement.2015.01.004.
[11] W. Liu, B. Tang, J. Han, X. Lu, N. Hu, Z. He, The structure healthy condition monitoring and fault diagnosis methods in wind turbines: a review, Renew. Sustain. Energy Rev. 44 (2015) 466–472, http://dx.doi.org/10.1016/j.rser.2014.12.005.

[12] B.G. Xu, Intelligent fault inference for rotating flexible rotors using Bayesian belief network, Expert Syst. Appl. 39 (2012) 816–822, http://dx.doi.org/10.1016/j.eswa.2011.07.079.
[13] V. Muralidharan, V. Sugumaran, Rough set based rule learning and fuzzy classification of wavelet features for fault diagnosis of monoblock centrifugal pump, Measurement 46 (2013) 3057–3063, http://dx.doi.org/10.1016/j.measurement.2013.06.002.
[14] H. Sim, R. Ramli, A. Saifizul, M. Abdullah, Empirical investigation of acoustic emission signals for valve failure identification by using statistical method, Measurement 58 (2014) 165–174, http://dx.doi.org/10.1016/j.measurement.2014.08.028.
[15] W. Caesarendra, B. Kosasih, A.K. Tieu, H. Zhu, C.A. Moodie, Q. Zhu, Acoustic emission-based condition monitoring methods: review and application for low speed slew bearing, Mech. Syst. Sig. Process. 72 (2016) 134–159, http://dx.doi.org/10.1016/j.ymssp.2015.10.020.
[16] R.F. Garcia, J.L.C. Rolle, M.R. Gomez, A.D. Catoira, Expert condition monitoring on hydrostatic self-levitating bearings, Expert Syst. Appl. 40 (2013) 2975–2984, http://dx.doi.org/10.1016/j.eswa.2012.12.013.
[17] Z. Xu, J. Xuan, T. Shi, B. Wu, Y. Hu, Application of a modified fuzzy ARTMAP with feature-weight learning for the fault diagnosis of bearing, Expert Syst. Appl. 36 (2009) 9961–9968, http://dx.doi.org/10.1016/j.eswa.2009.01.063.
[18] D. Dabrowski, Condition monitoring of planetary gearbox by hardware implementation of artificial neural networks, Measurement 91 (2016) 295–308, http://dx.doi.org/10.1016/j.measurement.2016.05.056.
[19] X. Jiang, S. Li, A dual path optimization ridge estimation method for condition monitoring of planetary gearbox under varying-speed operation, Measurement 94 (2016) 630–644, http://dx.doi.org/10.1016/j.measurement.2016.09.009.
[20] C. Li, R.-V. Sanchez, G. Zurita, M. Cerrada, D. Cabrera, R.E. Vásquez, Gearbox fault diagnosis based on deep random forest fusion of acoustic and vibratory signals, Mech. Syst. Sig. Process. 76 (2016) 283–293, http://dx.doi.org/10.1016/j.ymssp.2016.02.007.
[21] D. Dabrowski, Z. Hashemiyan, J. Adamczyk, A signal pre-processing algorithm designed for the needs of hardware implementation of neural classifiers used in condition monitoring, Measurement 73 (2015) 576–587, http://dx.doi.org/10.1016/j.measurement.2015.06.004.
[22] Y. Lei, J. Lin, M.J. Zuo, Z. He, Condition monitoring and fault diagnosis of planetary gearboxes: a review, Measurement 48 (2014) 292–305, http://dx.doi.org/10.1016/j.measurement.2013.11.012.
[23] Z. Li, Y. Jiang, C. Hu, Z. Peng, Recent progress on decoupling diagnosis of hybrid failures in gear transmission systems using vibration sensor signal: a review, Measurement 90 (2016) 4–19, http://dx.doi.org/10.1016/j.measurement.2016.04.036.
[24] H. Alkhadafe, A. Al-Habaibeh, A. Lotfi, Condition monitoring of helical gears using automated selection of features and sensors, Measurement 93 (2016) 164–177, http://dx.doi.org/10.1016/j.measurement.2016.07.011.
[25] N. Dayong, S. Changle, G. Yongjun, Z. Zengmeng, H. Jiaoyi, Extraction of fault component from abnormal sound in diesel engines using acoustic signals, Mech. Syst. Sig. Process. 75 (2016) 544–555, http://dx.doi.org/10.1016/j.ymssp.2015.10.037.
[26] J.-D. Wu, C.-H. Liu, Investigation of engine fault diagnosis using discrete wavelet transform and neural network, Expert Syst. Appl. 35 (2008) 1200–1213, http://dx.doi.org/10.1016/j.eswa.2007.08.021.
[27] S. Jafari, H. Mehdigholi, M. Behzad, Investigation of the relationship between engine valve leakage and acoustic emission measured on the cylinder head ignoring combustion effects, Proc. Inst. Mech. Eng., Part E: J. Process Mech. Eng. 230 (2016) 3–9, http://dx.doi.org/10.1177/0954408914527441.
[28] R. Losero, J. Lauber, T.-M. Guerra, Transmitted torque observer applied to real time engine and clutch torque estimation, IFAC-PapersOnLine 48 (2015) 73–78, http://dx.doi.org/10.1016/j.ifacol.2015.11.116.
[29] A. Rakotomamonjy, R. Le Riche, D. Gualandris, Z. Harchaoui, A comparison of statistical learning approaches for engine torque estimation, Control Eng. Pract. 16 (2008) 43–55, http://dx.doi.org/10.1016/j.conengprac.2007.03.009.
[30] S. Kermani, S. Delprat, T.-M. Guerra, R. Trigui, B. Jeanneret, Predictive energy management for hybrid vehicle, Control Eng. Pract. 20 (2012) 408–420, http://dx.doi.org/10.1016/j.conengprac.2011.12.001.
[31] T. Nüesch, M. Wang, P. Isenegger, C.H. Onder, R. Steiner, P. Macri-Lassus, L. Guzzella, Optimal energy management for a diesel hybrid electric vehicle considering transient PM and quasi-static NOx emissions, Control Eng. Pract. 29 (2014) 266–276, http://dx.doi.org/10.1016/j.conengprac.2014.01.020.
[32] D. Khiar, J. Lauber, T. Floquet, G. Colin, T.M. Guerra, Y. Chamaillard, Robust Takagi-Sugeno fuzzy control of a spark ignition engine, Control Eng. Pract. 15 (2007) 1446–1456, http://dx.doi.org/10.1016/j.conengprac.2007.02.003.
[33] B. Lee, G. Rizzoni, Y. Guezennec, A. Soliman, M. Cavalletti, J. Waters, Engine control using torque estimation, SAE Tech. Paper (2001), http://dx.doi.org/10.4271/2001-01-0995.
[34] J.J. Oh, S.B. Choi, J. Kim, Driveline modeling and estimation of individual clutch torque during gear shifts for dual clutch transmission, Mechatronics 24 (2014) 449–463, http://dx.doi.org/10.1016/j.mechatronics.2014.04.005.
[35] Z. Zhao, L. He, Y. Yang, C. Wu, X. Li, J.K. Hedrick, Estimation of torque transmitted by clutch during shifting process for dry dual clutch transmission, Mech. Syst. Sig. Process. 75 (2016) 413–433, http://dx.doi.org/10.1016/j.ymssp.2015.12.027.
[36] Y. Chamaillard, P. Higelin, A. Charlet, A simple method for robust control design, application on a non-linear and delayed system: engine torque control, Control Eng. Pract. 12 (2004) 417–429, http://dx.doi.org/10.1016/S0967-0661(03)00113-8.
[37] I. Ck, N. Mm, M.N. Cw, Prediction of marine diesel engine performance by using artificial neural network Model, J. Mech. Eng. Sci. (JMES) 10 (2016) 1917–1930, http://dx.doi.org/10.15282/jmes.10.1.2016.15.0183.
[38] N. Togun, S. Baysec, T. Kara, Nonlinear modeling and identification of a spark ignition engine torque, Mech. Syst. Sig. Process. 26 (2012) 294–304, http://dx.doi.org/10.1016/j.ymssp.2011.06.010.
[39] N.K. Togun, S. Baysec, Prediction of torque and specific fuel consumption of a gasoline engine by using artificial neural networks, Appl. Energy 87 (2010) 349–355, http://dx.doi.org/10.1016/j.apenergy.2009.08.016.
[40] E. Tosun, K. Aydin, M. Bilgili, Comparison of linear regression and artificial neural network model of a diesel engine fueled with biodiesel-alcohol mixtures, Alexandria Eng. J. 55 (2016) 3081–3089, http://dx.doi.org/10.1016/j.aej.2016.08.011.
[41] G. Najafi, B. Ghobadian, A. Moosavian, T. Yusaf, R. Mamat, M. Kettner, W. Azmi, SVM and ANFIS for prediction of performance and exhaust emissions of a SI engine with gasoline–ethanol blended fuels, Appl. Therm. Eng. 95 (2016) 186–203, http://dx.doi.org/10.1016/j.applthermaleng.2015.11.009.
[42] R. Douglas, J. Steel, R. Reuben, T. Fog, On-line power estimation of large diesel engines using acoustic emission and instantaneous crankshaft angular velocity, Int. J. Engine Res. 7 (2006) 399–410, http://dx.doi.org/10.1243/14680874JER00206.
[43] J. Franco, M.A. Franchek, K. Grigoriadis, Real-time brake torque estimation for internal combustion engines, Mech. Syst. Sig. Process. 22 (2008) 338–361, http://dx.doi.org/10.1016/j.ymssp.2007.08.002.
[44] F. Liu, G.A. Amaratunga, N. Collings, A. Soliman, An experimental study on engine dynamics model based in-cylinder pressure estimation, SAE Tech. Paper (2012), http://dx.doi.org/10.4271/2012-01-0896.
[45] T.R. Lin, A.C. Tan, L. Ma, J. Mathew, Estimating the loading condition of a diesel engine using instantaneous angular speed analysis, Eng. Asset Manage. Springer 2014 (2011) 259–272, http://dx.doi.org/10.1007/978-1-4471-4993-4_24.
[46] T. Aono, M. Saruwatari, J. Furuya, Estimation of engine torque and cylinder pressure index based on crankshaft rotation measurement, IFAC Proc. Vol. 46 (2013) 360–365, http://dx.doi.org/10.3182/20130904-4-JP-2042.00156.
[47] A. Stotsky, Adaptive estimation of the engine friction torque, Eur. J. Control 13 (2007) 618–624, http://dx.doi.org/10.3166/ejc.13.618-624.
[48] K. Nikzadfar, A.H. Shamekhi, More than one decade with development of common-rail diesel engine management systems: a literature review on modelling, control, estimation and calibration, Proc. Inst. Mech. Eng., Part D: J. Automob. Eng. 229 (2015) 1110–1142, http://dx.doi.org/10.1177/0954407014556114.
[49] P. Osinenko, M. Geißler, T. Herlitzius, S. Streif, Experimental results of slip control with a fuzzy-logic-assisted unscented Kalman filter for state estimation, in: Fuzzy Systems (FUZZ-IEEE), 2016 IEEE International Conference on, IEEE, 2016, pp. 501–507. https://doi.org/10.1109/FUZZ-IEEE.2016.7737728.
[50] A. Aguilera-González, J. Bosche, A. El Hajjaji, Unknown input estimation for diesel engine based on takagi-sugeno fuzzy descriptor systems, Am. Control Conf. (ACC) IEEE 2014 (2014) 3159–3164, http://dx.doi.org/10.1109/ACC.2014.6858949.
[51] J. Zhang, H. Lan, Fuzzy modeling of diesel engine based on working position, in: System Science and Engineering (ICSSE), 2012 International Conference on, IEEE, 2012, pp. 514–517. https://doi.org/10.1109/ICSSE.2012.6257238.
[52] L. Naderloo, H. Javadikia, M. Mostafaei, Modeling the energy ratio and productivity of biodiesel with different reactor dimensions and ultrasonic power using ANFIS, Renew. Sustain. Energy Rev. 70 (2017) 56–64, http://dx.doi.org/10.1016/j.rser.2016.11.035.
[53] N. Togun, S. Baysec, Nonlinear identification of a spark ignition engine torque based on ANFIS with NARX method, Expert Syst. 33 (2016) 559–568, http://dx.doi.org/10.1111/exsy.12172.
[54] X. Niu, C. Yang, H. Wang, Y. Wang, Investigation of ANN and SVM based on limited samples for performance and emissions prediction of a CRDI-assisted marine diesel engine, Appl. Therm. Eng. 111 (2017) 1353–1364, http://dx.doi.org/10.1016/j.applthermaleng.2016.10.042.
[55] B. Liu, J. Hu, F. Yan, R.F. Turkson, F. Lin, A novel optimal support vector machine ensemble model for NOx emissions prediction of a diesel engine, Measurement 92 (2016) 183–192, http://dx.doi.org/10.1016/j.measurement.2016.06.015.
[56] S. Shamshirband, M. Tabatabaei, M. Aghbashlo, L. Yee, D. Petković, Support vector machine-based exergetic modelling of a DI diesel engine running on biodiesel–diesel blends containing expanded polystyrene, Appl. Therm. Eng. 94 (2016) 727–747, http://dx.doi.org/10.1016/j.applthermaleng.2015.10.140.
[57] J. Martínez-Morales, E. Palacios, G.V. Carrillo, Modeling of internal combustion engine emissions by LOLIMOT algorithm, Proc. Technol. 3 (2012) 251–258, http://dx.doi.org/10.1016/j.protcy.2012.03.027.
[58] M. Castagné, S. Magand, F. Nicolas, Y. Bernard, C. Pailot, New calibration method and tool to minimize emissions on cold-start driving cycle, in: SIA International Conference: Diesel Powertrain, 2012, pp. 5–6.
[59] C. Bennett, J. Dunne, S. Trimby, D. Richardson, Engine cylinder pressure reconstruction using crank kinematics and recurrently-trained neural networks, Mech. Syst. Sig. Process. 85 (2017) 126–145, http://dx.doi.org/10.1016/j.ymssp.2016.07.015.
[60] M. Ouladsine, G. Bloch, X. Dovifaaz, Neural modelling and control of a Diesel engine with pollution constraints, J. Intell. Rob. Syst. 41 (2005) 157–171, http://dx.doi.org/10.1007/s10846-005-3806-y.
[61] S. Channapattana, A.A. Pawar, P.G. Kamble, Optimisation of operating parameters of DI-CI engine fueled with second generation Bio-fuel and development of ANN based prediction model, Appl. Energy 187 (2017) 84–95, http://dx.doi.org/10.1016/j.apenergy.2016.11.030.
[62] H.S. Saraee, H. Taghavifar, S. Jafarmadar, Experimental and numerical consideration of the effect of CeO_2 nanoparticles on diesel engine performance and exhaust emission with the aid of artificial neural network, Appl. Therm. Eng. 113 (2017) 663–672, http://dx.doi.org/10.1016/j.applthermaleng.2016.11.044.
[63] H. Taghavifar, H. Taghavifar, A. Mardani, A. Mohebbi, S. Khalilarya, S. Jafarmadar, Appraisal of artificial neural networks to the emission analysis and prediction of

CO_2, soot, and NO_x of n-heptane fueled engine, J. Cleaner Prod. 112 (2016) 1729–1739, http://dx.doi.org/10.1016/j.jclepro.2015.03.035.
[64] G. Kökkülünk, E. Akdoğan, V. Ayhan, Prediction of emissions and exhaust temperature for direct injection diesel engine with emulsified fuel using ANN, Turk. J. Electr. Eng. Comput. Sci. 21 (2013) 2141–2152, http://dx.doi.org/10.3906/elk-1202-24.
[65] Y. Cay, Prediction of a gasoline engine performance with artificial neural network, Fuel 111 (2013) 324–331, http://dx.doi.org/10.1016/j.fuel.2012.12.040.
[66] F. Rahimi-Ajdadi, Y. Abbaspour-Gilandeh, Artificial neural network and stepwise multiple range regression methods for prediction of tractor fuel consumption, Measurement 44 (2011) 2104–2111, http://dx.doi.org/10.1016/j.measurement.2011.08.006.
[67] H. Oğuz, I. Sarıtas, H.E. Baydan, Prediction of diesel engine performance using biofuels with artificial neural network, Expert Syst. Appl. 37 (2010) 6579–6586, http://dx.doi.org/10.1016/j.eswa.2010.02.128.
[68] M.-L. Huang, Y.-H. Hung, Z.-S. Yang, Validation of a method using Taguchi, response surface, neural network, and genetic algorithm, Measurement 94 (2016) 284–294, http://dx.doi.org/10.1016/j.measurement.2016.08.006.
[69] S. Kumar, P.S. Pai, B.S. Rao, G. Vijay, Prediction of performance and emission characteristics in a biodiesel engine using WCO ester: a comparative study of neural networks, Soft. Comput. 20 (2016) 2665–2676, http://dx.doi.org/10.1007/s00500-015-1666-9.
[70] A. Rohani, M.H. Abbaspour-Fard, S. Abdolahpour, Prediction of tractor repair and maintenance costs using artificial neural network, Expert Syst. Appl. 38 (2011) 8999–9007, http://dx.doi.org/10.1016/j.eswa.2011.01.118.
[71] Y. Ge, Y. Huang, D. Hao, G. Li, H. Li, An indicated torque estimation method based on the Elman neural network for a turbocharged diesel engine, Proc. Inst. Mech. Eng., Part D: J. Automob. Eng. 230 (2016) 1299–1313, http://dx.doi.org/10.1177/0954407015606271.
[72] M. Bietresato, A. Calcante, F. Mazzetto, A neural network approach for indirectly estimating farm tractors engine performances, Fuel 143 (2015) 144–154, http://dx.doi.org/10.1016/j.fuel.2014.11.019.
[73] E. Grünbacher, P. Kefer, L. Del Re, Estimation of the mean value engine torque using an extended Kalman filter, SAE Tech. Paper (2005), http://dx.doi.org/10.4271/2005-01-0063.
[74] Y. Zweiri, L. Seneviratne, Diesel engine indicated and load torque estimation using a non-linear observer, Proc. Inst. Mech. Eng., Part D: J. Automob. Eng. 220 (2006) 775–785, http://dx.doi.org/10.1243/09544070JAUTO48.
[75] Y.H. Zweiri, D. Seneviratne, Diesel engine indicated torque estimation based on artificial neural networks, in: Computer Systems and Applications, 2007. AICCSA'07. IEEE/ACS International Conference on, IEEE, 2007, pp. 791–798. https://doi.org/10.1109/AICCSA.2007.370723.
[76] A.-M. Shamekhi, A.H. Shamekhi, A new approach in improvement of mean value models for spark ignition engines using neural networks, Expert Syst. Appl. 42 (2015) 5192–5218, http://dx.doi.org/10.1016/j.eswa.2015.02.031.
[77] S. Tasdemir, I. Saritas, M. Ciniviz, N. Allahverdi, Artificial neural network and fuzzy expert system comparison for prediction of performance and emission parameters on a gasoline engine, Expert Syst. Appl. 38 (2011) 13912–13923, http://dx.doi.org/10.1016/j.eswa.2011.04.198.
[78] M.K.D. Kiani, B. Ghobadian, T. Tavakoli, A. Nikbakht, G. Najafi, Application of artificial neural networks for the prediction of performance and exhaust emissions in SI engine using ethanol-gasoline blends, Energy 35 (2010) 65–69, http://dx.doi.org/10.1016/j.energy.2009.08.034.
[79] T.F. Yusaf, D. Buttsworth, K.H. Saleh, B. Yousif, CNG-diesel engine performance and exhaust emission analysis with the aid of artificial neural network, Appl. Energy 87 (2010) 1661–1669, http://dx.doi.org/10.1016/j.apenergy.2009.10.009.
[80] B. Ghobadian, H. Rahimi, A. Nikbakht, G. Najafi, T. Yusaf, Diesel engine performance and exhaust emission analysis using waste cooking biodiesel fuel with an artificial neural network, Renew. Energy 34 (2009) 976–982, http://dx.doi.org/10.1016/j.renene.2008.08.008.
[81] G. Najafi, B. Ghobadian, T. Tavakoli, D. Buttsworth, T. Yusaf, M. Faizollahnejad, Performance and exhaust emissions of a gasoline engine with ethanol blended gasoline fuels using artificial neural network, Appl. Energy 86 (2009) 630–639, http://dx.doi.org/10.1016/j.apenergy.2008.09.017.
[82] H.S. Yücesu, A. Sozen, T. Topgül, E. Arcaklioğlu, Comparative study of mathematical and experimental analysis of spark ignition engine performance used ethanol–gasoline blend fuel, Appl. Therm. Eng. 27 (2007) 358–368, http://dx.doi.org/10.1016/j.applthermaleng.2006.07.027.
[83] M. Gölcü, Y. Sekmen, P. Erduranlı, M.S. Salman, Artificial neural-network based modeling of variable valve-timing in a spark-ignition engine, Appl. Energy 81 (2005) 187–197, http://dx.doi.org/10.1016/j.apenergy.2004.07.008.
[84] J. Chauvin, G. Corde, P. Moulin, M. Castagné, N. Petit, P. Rouchon, Real-time combustion torque estimation on a diesel engine test bench using time-varying Kalman filtering, in; Decision and Control, 2004. CDC. 43rd IEEE Conference on, IEEE, 2004, pp. 1688–1694. https://doi.org/10.1109/CDC.2004.1430287.
[85] R.F. Turkson, F. Yan, M.K.A. Ali, J. Hu, Artificial neural network applications in the calibration of spark-ignition engines: an overview, Eng. Sci. Technol. Int. J. 19 (2016) 1346–1359, http://dx.doi.org/10.1016/j.jestch.2016.03.003.
[86] J. Rezaei, M. Shahbakhti, B. Bahri, A.A. Aziz, Performance prediction of HCCI engines with oxygenated fuels using artificial neural networks, Appl. Energy 138 (2015) 460–473, http://dx.doi.org/10.1016/j.apenergy.2014.10.088.
[87] A. Sharma, V. Sugumaran, S.B. Devasenapati, Misfire detection in an IC engine using vibration signal and decision tree algorithms, Measurement 50 (2014) 370–380, http://dx.doi.org/10.1016/j.measurement.2014.01.018.
[88] W.K. Yap, V. Karri, Emissions predictive modelling by investigating various neural network models, Expert Syst. Appl. 39 (2012) 2421–2426, http://dx.doi.org/10.1016/j.eswa.2011.08.091.
[89] R. Manjunatha, P.B. Narayana, K.H.C. Reddy, K.V.K. Reddy, Radial basis function neural networks in prediction and modeling of diesel engine emissions operated for biodiesel blends under varying operating conditions, Indian J. Sci. Technol. 5 (2012) 2307–2312.
[90] J. Wang, Y. Zhang, Q. Xiong, X. Ding, NOx prediction by cylinder pressure based on RBF neural network in diesel engine, in: Measuring Technology and Mechatronics Automation (ICMTMA), 2010 International Conference on, IEEE, 2010, pp. 792–795. https://doi.org/10.1109/ICMTMA.2010.621.
[91] J.-D. Wu, P.-H. Chiang, Y.-W. Chang, Y.-J. Shiao, An expert system for fault diagnosis in internal combustion engines using probability neural network, Expert Syst. Appl. 34 (2008) 2704–2713, http://dx.doi.org/10.1016/j.eswa.2007.05.010.
[92] M.R. Ghotbi, M.R. Monazzam, N. Khanjani, F. Nadri, S.M.B. Fard, Driver exposure and environmental noise emission of Massey Ferguson 285 tractor during operations with different engine speeds and gears, Afr. J. Agric. Res. 8 (2013) 652–659.
[93] ASME, Reciprocating Internal-Combustion Engines: Performance Test Codes (PTC), American Society of Mechanical Engineers, 2012, pp. 1–33.
[94] M. Canakci, A.N. Ozsezen, E. Arcaklioglu, A. Erdil, Prediction of performance and exhaust emissions of a diesel engine fueled with biodiesel produced from waste frying palm oil, Expert Syst. Appl. 36 (2009) 9268–9280, http://dx.doi.org/10.1016/j.eswa.2008.12.005.
[95] OECD, OECD Standard Code for the Official Testing of Agricultural and Forestry Tractor Performance, Organisation for Economic Co-operation and Development, 2012, pp. 1–91.
[96] N.S. Sarvestani, A. Rohani, A. Farzad, M.H. Aghkhani, Modeling of specific fuel consumption and emission parameters of compression ignition engine using nanofluid combustion experimental data, Fuel Process. Technol. 154 (2016) 37–43, http://dx.doi.org/10.1016/j.fuproc.2016.08.013.
[97] S.H. Al-lwayzy, T. Yusaf, Diesel engine performance and exhaust gas emissions using Microalgae Chlorella protothecoides biodiesel, Renew. Energy 101 (2017) 690–701, http://dx.doi.org/10.1016/j.renene.2016.09.035.
[98] C. Borgnakke, R.E. Sonntag, Fundamentals of Thermodynamics, eighth ed., Wiley, New York, USA, 2012.
[99] L. Zhen-Tao, F. Shao-mei, Study of CNG/diesel dual fuel engine's emissions by means of RBF neural network, J. Zhejiang Univ.-SCIENCE A 5 (2004) 960–965.